Cluster-based Reduced-Order Modeling to Capture Intermittent Dynamics of Interacting Wakes

Tyler P. Dare* and Zachary P. Berger†
Applied Research Laboratory, Pennsylvania State University, State College, PA 16804

Michael Meehan‡
Mechanical Engineering, University of Colorado - Boulder, Boulder, CO, 80309

Jacqueline O'Connor§
Mechanical Engineering, Pennsylvania State University, University Park, PA, 16802

Interacting flows are found in a range of aviation-relevant technologies, including flow control devices, engine combustors and augmentors, and aerodynamic control surfaces. The structure and dynamics of interacting jets and wakes, including both large-scale coherent dynamics and turbulent fluctuations, is fundamentally different from that of a single flowfield. The goal of this work is to understand large-scale, intermittent dynamics of turbulent interacting wakes and jets using an improved reduced-order modeling strategy, cluster-based reduced-order modeling (CROM), to capture these dynamics. We compare the dynamics of a three-wake system at two spacings to that of a single wake flowfield using the cluster-based method. The CROM is able to capture the expected dynamics of the single wake, and the results are analogous to those from proper orthogonal decomposition. However, CROM reveals a much more complicated set of dynamics in the interacting wake cases, including the existence of two sets of dynamics that intermittently appear and the switching points between them, that the POD was unable to detect. CROM is used to quantify these dynamics and understand the effect of bluff-body spacing on the three-wake flowfields.

Nomenclature

D = diameter of the bluff body $[m]$

D_{ij} = distance metric $[m/s]$

f = characteristic frequency $[Hz]$

k = number of snapshots

P_{jk} = probability of transfer between centroid j and k

*Assistant Research Professor, Applied Research Laboratory, Pennsylvania State University.
†Assistant Research Professor, Applied Research Laboratory, Pennsylvania State University, AIAA Member.
‡Graduate Research Assistant, Mechanical Engineering, University of Colorado, Boulder, AIAA Student Member.
§Assistant Professor, Mechanical Engineering, Pennsylvania State University, AIAA Member.

Re = Reynolds number

s = gap width between the two bluff bodies $[m]$

U_b = mixture bulk flow velocity $[m/s]$

u_o = freestream velocity $[m/s]$

w = center-to-center spacing of the bluff bodies $[m]$

θ = momentum thickness $[m]$

ν = mixture viscosity $[m^2/s]$

I. Introduction

The dynamics of single wakes and single jets, here described as "unit flows," have been the subject of intense study for decades. Generally, these efforts considered large-scale motions, generated by the hydrodynamic instabilities present in the flowfield, or the turbulent characteristics of these flows. However, the dynamics of interacting flows have not been considered as extensively, despite the importance of interacting flows in a number of aerospace technologies, including flow control devices and aircraft engine combustors. In this study, we consider the dynamics of three interacting wakes using a novel cluster-based reduced order modeling (CROM) to quantify the intermittency and dynamical shifts seen in these flows.

The dynamics of multi-wake systems have been investigated in a number of contexts, where early investigators, including Biermann and Herrnstein [1] and Spivack [2], were particularly interested in the dynamics of flow around two cylinders, which were meant to mimic the flow around pairs of skyscrapers or pier pillars in the ocean. These early studies focused on the drag coefficient of the two-body system at different body spacings, and comparing it to that of the single-wake system. Their results showed that the system displayed bi-modal dynamics, where the drag coefficient would intermittently flip between two values. Interestingly, the average of these two values was typically less than the drag coefficient of a single body, indicating the importance that wake interaction plays on flowfield structure and dynamics.

These early studies inspired further literature on dual-wake systems, including works by Sumner et al. [3], Le Gal and coworkers [4, 5], Kiya *et al.* [6], Yen and Liu [7], Kim and Durbin [8], Bearman and Wadcock [9], Wang and Zhou [10], Carini *et al.* [11–13], and Hayashi *et al.* [14]. Many of these studies focused on low-Reynolds number regimes ($Re \sim$ O(100)), where detailed observation of the structure and dynamics of multi-wake systems was possible. It was found that dual-wake systems often displayed a "bias" in the wake structure, particularly at close spacings, where the wake behind one body was larger than the other. This bias caused the jet flow between the two bodies to deflect towards the smaller-wake body, altering the time-averaged flow structure downstream of the two-wake system.

The main focus of this previous work was the impact of body spacing on the vortex shedding behind the two bluff

bodies. Alam *et al.* [15] summarized the dynamics into three spacing regimes: close, intermediate, and far spacings, where spacing is typically quantified using the bluff-body spacing, w, normalized by the bluff-body diameter, D. The vortex shedding in the close ($w/D < 2.2$) and far ($w/D > 3$) regimes showed relatively regular vortex shedding. In addition to vortex shedding in the close regime, the flowfield displayed a "flip-flopping" motion, where a bias in the flow flipped on a timescale longer than the vortex shedding timescales. The dynamics in the intermediate-spacing regime were found to be highly intermittent, with no dominant vortex shedding frequency.

Studies of more than two bluff bodies are limited. Work by Sumner *et al.* [3] provided an overview of the time-averaged structure of three-wake systems and some discussion of the dynamics. More recent work by Zheng and Alam [16] considered very low Reynolds numbers ($Re = 150$) flow dynamics behind three bluff bodies. Hayashi *et al.* [14] investigated systems with up to five flat plates at a large range of Reynolds numbers ($Re = 6000 - 19000$), but their focus was mostly on time-averaged flow structure. The limited results from previous studies of systems with more than three bluff bodies leaves significant questions as to the dynamics of these systems.

One of the key findings from these studies is that intermittency is inherent in multi-wake systems, and the intermittency has not been quantified in these flowfields. Turbulent flows encompass a large range of length and time scales, evolving in three-dimensional space as well as in time. In working to interpret these complex flow physics, techniques that reduce the complexity of the problem are beneficial. Recent work by Meehan *et al.* [17] used statistical analysis of the data discussed in this paper to describe the intermittency. In this work, some more traditional analysis methods (POD and phase-resolved analysis) were used to investigate this three bluff-body flow. These techniques, however, did a poor job of identifying the multi-modal behavior present at certain conditions. To address this, we used the Hilbert transform to calculate the instantaneous frequency and phase of oscillations within the shear layers of these bluff bodies. Probability density functions were used to quantify the distribution of these instantaneous phases between vortex shedding from three adjacent wakes at a range of spacings. It was found that certain spacings resulted in highly coherent phase relationships, whereas other spacings produced almost uniform distributions of vortex-shedding phases, indicating that the flow behaved randomly at these conditions. While this statistical description is a useful way of quantifying the behavior of the system, it does not provide much detail as to the physics of mode switching or the reason behind different vortex-shedding phases. Reduced-order modeling (ROM) provides a methodology for decomposing a quantity into its fundamental dynamics or "modes."

Depending on the ultimate goal of the model, the decomposition can be truncated to include only modal contributions of interest. This methodology of developing a low-dimensional representation of a given quantity is especially useful in the context of real-time, closed-loop flow control. Reduced-order modeling can be implemented to extract the most important features of the flow to achieve the particular control objective of interest, and begin to interpret the flow physics from a high level. Perhaps the most widely used modal decomposition with respect to turbulent flows is the proper orthogonal decomposition (POD), sometimes also known as principal component analysis (PCA). This technique

is also commonly used in the fields of image processing, data compression, optimal control, and signal analysis, among others. The POD was first introduced into the turbulence community in 1967 by John Lumley [18]. At the time, many researchers were studying large-scale coherent structures present in turbulent flowfields. This prompted a desire to develop a quantitative representation of the large-scale motion. Since the POD is an energy based decomposition, it is ideal for identifying the differences in large- and small-scale structures in the context of turbulent flows. Here, the POD provides a basis set that maximizes the overall turbulent kinetic energy. This is done by solving an eigenvalue problem on the two-point correlation tensor of the velocity field. The details of the POD can be found in the work of Berkooz *et al.* [19].

Over the years, there have been several variations on the original implementation of the POD (sometimes known as the classical POD), to account for improvements in data processing and advancement in measurement techniques. For example, in 1987, Sirovich [20] introduced the snapshot method for POD by which the formulation of the problem is done temporally, rather than spatially. The kernel of the eigenvalue problem becomes the two-time correlation tensor of the velocity field. This is particularly useful when the number of grid points in the flow field is substantially greater than the number of flow realizations, as is commonly the case with particle image velocimetry (PIV) data sets. Some other eigenmode decompositions have been successfully implemented in recent years to gain a deeper understanding of complex flow physics in turbulent fields. These techniques include the balanced POD (BPOD) [21, 22], split-POD [23] , and dynamic mode decomposition (DMD) [24].

Recently, Kaiser *et al.* [25] have introduced a method of reduced-order modeling of flows using a cluster analysis technique, called Cluster-based Reduced Order Modeling (CROM). Essentially, velocity snapshots are segmented into a small number of groups, with each group of snapshots having a similar velocity field. The groups are assigned via the k-means clustering algorithm [26]. The algorithm produces a collection of k snapshot centroids (with k generally on the order of 10), with the goal of maximizing the similarity between each of the measured snapshots and its most similar snapshot centroid. Once each snapshot has been assigned to a centroid, a transition matrix can be calculated. The transition matrix describes the probability that each of the k different states transition to one another. For example, snapshots in cluster 2 might transition to cluster 7 with 30% probability.

The CROM approach is a powerful way to simplify the dynamics of a complex system and investigate the causes of intermittency. In the original study, Kaiser *et al.* [25] applied the CROM method to simulations of a two-dimensional mixing layer at $Re = 500$ and to the Ahmed body (a general vehicle shape) at $Re = 30,000$. For the mixing layer, CROM was used to separate vortex pairing events from Kelvin-Helmholtz instabilities and identify a cluster representing transition between the two flow regimes. For the vehicle model, CROM was used to distinguish between two main flow states and to find a transition state between the two. The vehicle model is a particularly interesting example, since it demonstrates that using the CROM method can give useful results at high Reynolds numbers.

In a subsequent study by Östh *et al.* [27], CROM was applied to a large-eddy simulation (LES) of a high-speed

train. Two major flow states were found, including in-phase and out-of-phase oscillations of two vortices behind the train. Again, CROM also identified transition clusters between the major groups. Given that the out-of-phase group experienced lower drag than the in-phase group, CROM could potentially be exploited to develop flow control aimed at drag reduction. The first experimental use of the CROM method was by Cao *et al.* [28], who studied cycle-to-cycle variations in internal combustion engines. The results were used to show that the breakdown of the large-scale coherent tumbling motion can be predicted at an earlier point in the cycle. The authors suggest that the results of CROM analysis can be used to develop control schemes to improve engine stability and efficiency.

This progress in CROM indicates that it is a promising technique for capturing intermittency in interacting flows. This work shows the potential use of CROM for these complicated shear flows. The remainder of this paper is organized as follows. First, we describe the experimental configuration and the implementation of the CROM algorithm. Next, we describe the time-averaged structure of the flowfield, and then describe the flow dynamics using a traditional ROM method, POD. Then we implement the CROM technique, showing key transitions between different flow states in a number of interacting flow configurations.

II. Experimental Overview

The experimental facility consists of an open flow facility with a 12 in. by 4 in. rectangular exit plane and 4 in. long bluff-bodies with equilateral triangular cross-sections. The configuration permits the formation of statistically two-dimensional flowfields, allowing the use of planar laser-based diagnostics as out-of-plane motions can be neglected. Futhermore, the facility is highly modular such that it can be operated with a single bluff-body or multiple bluff-bodies with variable spacings A schematic is shown in Figure 1. More details about the facility can be found in recent work by Meehan *et al.* [17]. In this work, the Reynolds number, defined in Equation (1), is held fixed at 4000:

$$Re = \frac{U_b D}{\nu} \tag{1}$$

where U_b, D and ν are the mixture bulk flow velocity at the exit, the bluff-body diameter and the mixture viscosity respectively. Flow conditioning is achieved through two sections of 4 inch thick, 1/8 inch cell diameter honeycomb to ensure uniform flow at the exit plane. A metal perforated plate located 6 inches below the experiment exit acts as a passive turbulence generator. The volume flow rates of the air is measured with a Thermal Instrument Model 600-9/9500P digital flow meter. Spacing distance, w, between the three triangular bluff bodies was varied, as is shown in Figure 1.

Velocity field measurements were performed using high-speed particle image velocimetry. The flow field is seeded with sub-micron sized aluminum oxide particles, and illuminated with 532 nm light from a Quantronix Hawk-Duo Nd:YAG dual cavity laser operating at 4 kHz. A Photron SA-5 camera, also running at 4 kHz, was used to image the

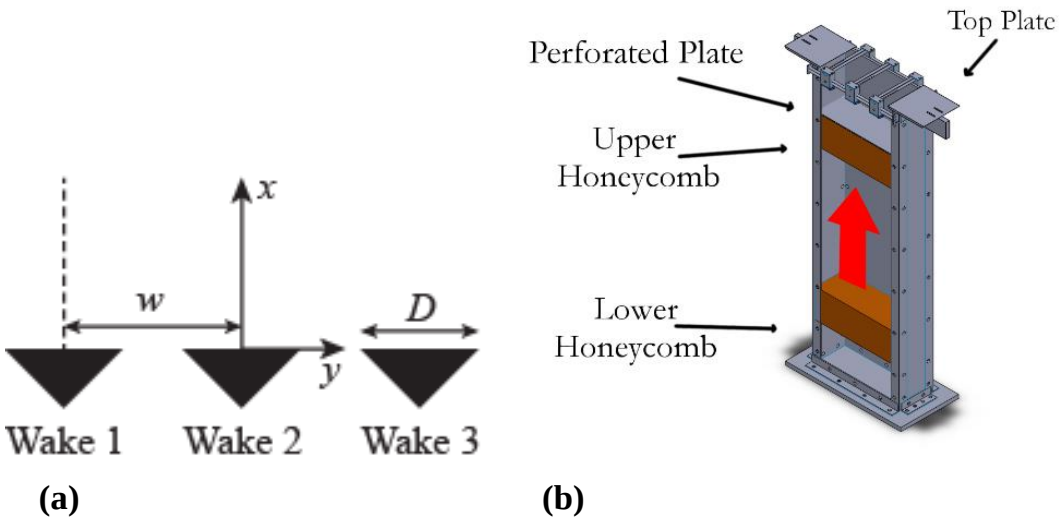

Fig. 1 Schematic (a) and drawing (b) of experimental configuration

seeded flow field, resulting in a spatial resolution of 0.129 mm. PIV calculations were performed using DaVis 8.3 from LaVision. For each case, 5001 images are acquired at a data acquisition rate of 4 kHz. The raw seeded images are first preprocessed using a 5 frame sliding minimum filter. The vector fields are calculated by using an multi-pass algorithm where the first pass is performed with an interrogation window size of 64x64 and 50% overlap while the final two passes are performed with a 16x16 window size with 50% overlap. Post-processing of vectors in DaVis includes a universal outlier detection scheme with a 3x median filter. This ensures removal of groups with less than 5 vectors and vectors with a residual greater than 2. It also ensures re-insertion of vectors with a residual less than 3. The average number of vectors replaced per dataset range from 5% to less than 7% and the percent first choice vectors are between 88% and 93% for the datasets analyzed in this paper.

III. CROM Methodology

The CROM method is a way of identifying important dynamics in systems with intermittent behavior. The method can be separated into two stages. First, groups of similar snapshots are found using the k-means clustering algorithm. Then, the cluster assignments are used to determine the transition probabilities between each group. During the clustering stage of CROM, snapshots are grouped using the k-means algorithm. The goal of this clustering is that snapshots that are similar are placed in the same group, with "similarity" defined by an appropriate distance metric. For CROM, the distance metric between snapshot i and snapshot j is chosen to be the L^2 norm instantaneous velocity fields,

$$D_{ij} = \left\| \bar{v}_i - \bar{v}_j \right\|_2 . \tag{2}$$

Two snapshots i and j are similar if their distance D_{ij} is low. Other distance metrics can be chosen, such as the L^1 norm or the maximum 2-D cross-correlation, but the L^2 norm metric seems to give satisfactory results in previous studies [25][27]. Calculating the full distance matrix is computationally expensive for large numbers of snapshots. Instead, the k-means algorithm uses an iterative method to optimize the assignments of snapshots into k groups, such that the total distances of each snapshot to its group's centroid is minimized [26]. For each iteration, only the distance between each snapshot and each centroid needs to be calculated. The number of centroids, k, must be chosen by the analyst, but it is typically much less than the number of snapshots. The output of the k-means algorithm is the group assignments of each snapshot and the centroid of each group. Each centroid is the mean velocity field of each snapshot in its group.

The number of clusters for each of the cases in this work was determined by a multi-step method. For each case, the clustering algorithm was performed using a varying number of clusters, up to 30. Then, the total variance with k clusters was calculated as

$$\sigma_k^2 = \sum_{j=1}^{k} \sum_{i=1}^{n_j} \left\| \bar{v}_i - \bar{v}_{c_j} \right\|_2^2, \tag{3}$$

where n_j is the number of snapshots $\bar{v}_i$ in cluster j, and $\bar{v}_{c_j}$ is the centroid of cluster j. The percent of total variance that is explained by clustering with k clusters is then given by

$$1 - \sigma_k^2 / \sigma_1^2, \tag{4}$$

where σ_1^2 is the variance of the entire data set (the single cluster case). The percent of variance explained for each case and up to 30 clusters is shown in Figure 2. The amount of variance explained approaches 100% as the number of clusters approaches the number of snapshots. For the three-body cases, the percent of variance explained is higher than the single-body case. This is likely due to the complexity of the flowfields and the normalization by the variance of the original data; for complex flowfields, even a small number of clusters is a significant improvement over the single cluster case.

To determine an appropriate number to use, a knee was found in the explained variance graphs. The knee was defined by the point that maximizes the average R^2 statistic between best-fit lines through cluster numbers below and above that point. The optimal number of clusters and resulting best-fit lines for each case are shown in Figure 2.

This calculation results in a different optimal number of clusters for each case: five clusters for the single bluff body, 10 clusters for the $w/D = 1.94$ spacing, and nine clusters for the $w/D = 2.99$ spacing. Despite the slight difference in the optimal number of clusters for the three bluff-body cases, we decided to use 10 clusters for analyzing both to keep some consistency between the two cases. The five clusters are used for the single bluff-body data, however, as the dynamics are significantly more simple.

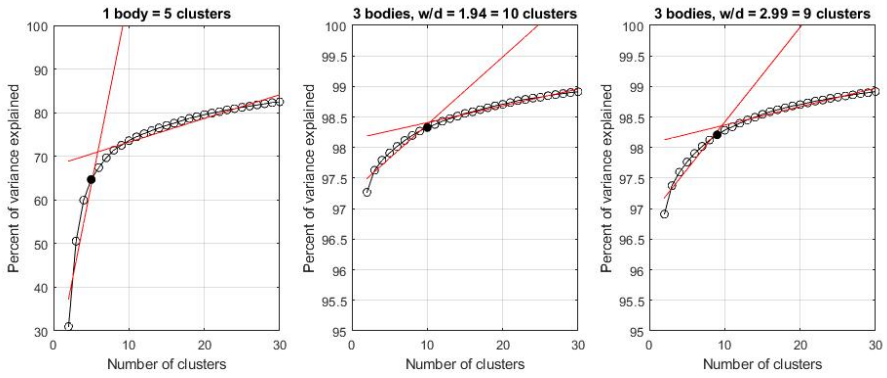

Fig. 2 Percent variance vs. number of clusters for three cases.

After the k-means analysis is complete, the cluster assignments are used to examine transitions between groups of snapshots. A transition probability matrix, T_{ij}, is generated by counting the number of times a snapshot in group i is followed by a snapshot in group j and dividing by the total amount of snapshots in group i. The diagonal entries in T_{ij} are typically high, since two adjacent snapshots are likely to be placed in the same group. However, the off-diagonal entries contain more interesting dynamics. If a row of T_{ij} contains exactly one off-diagonal entry, then the flow state represented by cluster i always transitions to the flow state represented by the non-zero off-diagonal entry. A single non-zero off-diagonal entry for each row would be typical of cyclic flow, such as vortex shedding. However, if there are multiple non-zero off-diagonal entries for row i, the flow state represented by cluster i can be thought of as a transition state, in which the dynamics can evolve into one of many subsequent states. Analysis of the cluster centroids and transition probability matrix can give insight into complex, intermittent flow dynamics.

IV. Results

A. Time-averaged flowfield structure

The time-averaged axial velocity (Figure 3) is shown for three cases: a single wake, three wakes at $w/D = 1.94$, and three wakes at $w/D = 2.99$. A number of features change when comparing the single-wake case to the three-wake cases. The most striking change is the difference in the recirculation zone downstream of the bluff bodies. The recirculation zone at $w/D = 1.94$ has a similar maximum recirculation velocity to that of the single-wake case, although the velocity deficit zone in the three-wake case is longer than that of the single-wake case. In the three-wake case with $w/D = 2.99$, the recirculation strength is reduced significantly and the velocity deficit zone is much longer than in either the single- or three-wake case at $w/D = 1.94$. This trend of decreasing recirculation zone strength and increasing recirculation zone size is monotonic between the two three-wake cases, although they are not shown here for brevity. Additionally, bending of the jets between the bluff bodies is observed in the three-wake cases; the jets bend in towards the centerline of the flowfield. This bending has been observed in previous studies of dual-jets [29]. Although not visible in the field of

view in Figure 3, the jets on the outer sides of the left and right bluff bodies also bend inwards, likely as a result of the quiescent boundary condition on either side of the experiment. It should be noted that many previous multi-bluff-body experiments in the literature look at systems in wind or water tunnels, which creates a very different boundary condition on the flow than the current open configuration does. We have discussed the significant implications for this difference in our previous work [17].

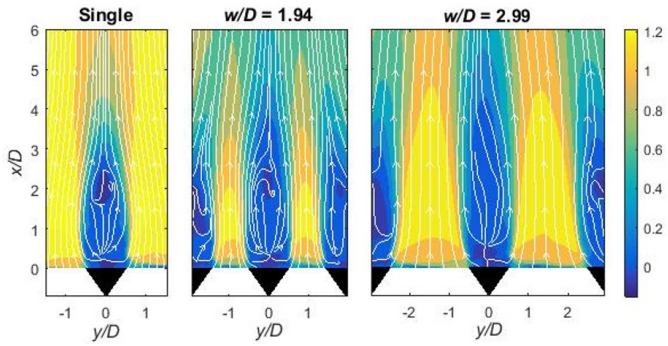

Fig. 3 Time-averaged axial velocity profiles of single wake (left), and three wakes at $w/D = 1.68$ (center) and $w/D = 2.2$ (right)

The velocity RMS (comprised of two components of velocity from the 2D PIV) is shown in Figure 4. The RMS downstream of the bluff body in the single-wake case is large, which is the result of the coherent, asymmetric wake vortex shedding that takes place in that region; this is the Bénard von Kármán (BVK) wake instability. The RMS levels of the three-wake cases are lower, even in the regions downstream of the bluff bodies, as a result of the reduction in vortex-shedding coherence. Previous work by Meehan *et al.* [17] details the statistics of this vortex shedding in these cases, clearly indicating the statistical nature of the vortex shedding. The CROM analysis will also show that the vortex shedding in these regions is more intermittent, which results in a lower RMS velocity, and will more clearly highlight the dominant flow structures that drive this intermittency.

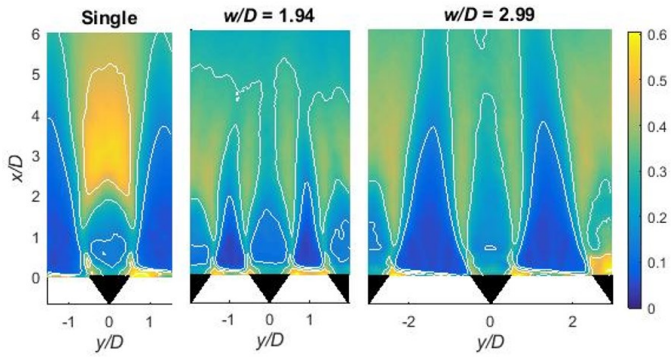

Fig. 4 RMS velocity profiles of single wake (left), and three wakes at $w/D = 1.68$ (center) and $w/D = 2.2$ (right)

B. Single-wake dynamics

The dynamics of the single-wake case are discussed first in order to establish a baseline for the three-wake analysis. In particular, we focus on the comparison of the POD and CROM results, as the dynamics of a single bluff-body flowfield are well documented [30], in order to identify the valuable insight that CROM provides. The vorticity of the first ten POD modes for the single bluff body case are shown in Figure 5. The first two modes of the POD capture the motion of the wake undergoing the Bénard von Kármán instability. Two modes are required to capture this motion as it convects; the convection is evident from the phase shift of the oscillations in mode 2 relative to mode 1. The source of modes 3-9 are not completely evident, but mode 10 likely captures the vortex motion in the shear layers. Further inspection of modes higher than 10 shows significant shear layer motion for a large number of modes; while the number of modes with shear layer motion is large, the energy contained in these modes is not.

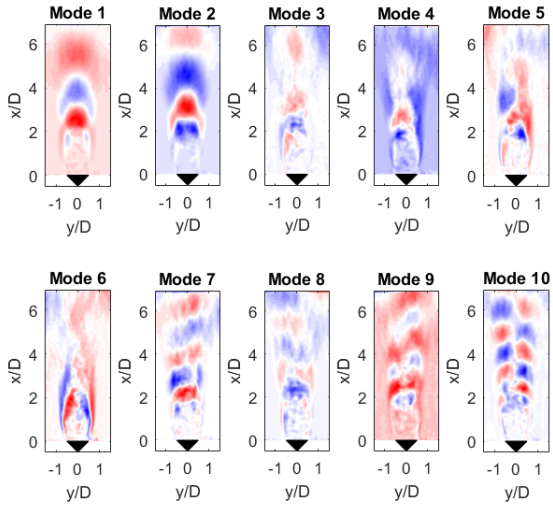

Fig. 5 Vorticity for the first ten POD modes for single bluff body case.

The results of the clustering process for the single bluff body case are shown in Figure 6. The system cycles between five clusters, all of which show the structure of the Bénard von Kármán wake vortex shedding. Each of the cluster centroids pictured are similarly structured but display convection from one centroid to the next, which is representative of the downstream convection of the coherent structures.

The repeatability in the flowfield can also be observed by plotting the cluster index assignments as a function of time, as is shown in Figure 7. For the entire measurement time, the system oscillates between these five clusters. The choice of a different number of clusters does reveal slightly different dynamics. For example, the use of 10 clusters (twice the optimal) results in eight clusters that resemble the wake shedding mode, and two that display slightly different dynamics. However, these two different clusters have a very small transition probability and the system spends almost no time in these clusters. In a case where the dynamics are strongly oscillatory and repeatable, the number of clusters

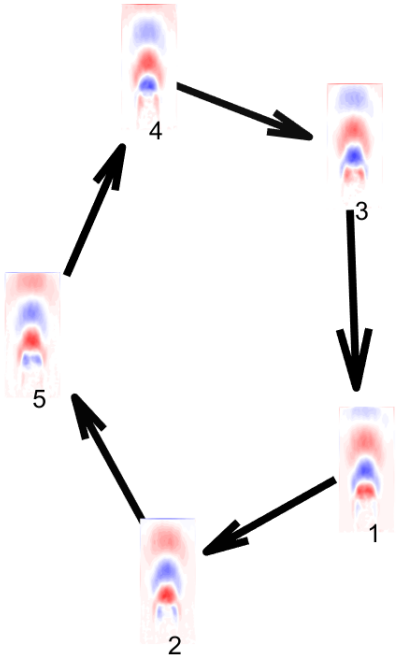

Fig. 6 Transition diagram with vorticity of cluster centroids.

used for the CROM does not greatly change the interpretation of the dynamics. However, use of the optimal number of clusters is important for systems with more complex dynamics, which is why a larger number of clusters are chosen for the three-body cases.

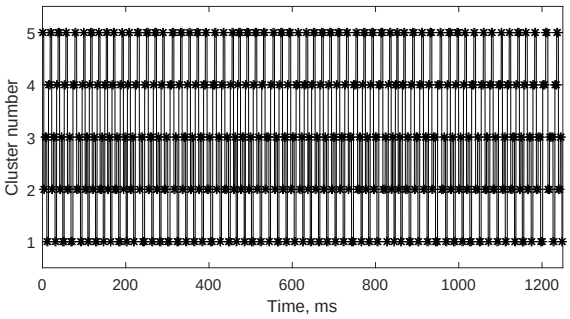

Fig. 7 Snapshot cluster assignments for single bluff body case.

C. $w/D = 2.99$

We present the dynamics of the $w/D = 2.99$ next because it shows how CROM response to a flowfield with multiple coherent oscillations. The transfer diagram with the streamwise component of all cluster centroids for the $w/D = 2.99$ case is shown in Figure 8. The POD results from this case, discussed in Meehan *et al.* [17], show pairs of modes with

outer wake oscillations (modes 1 and 2) and center wake oscillations (modes 3 and 4), and a large number of low-energy modes with oscillations in the shear layers shed from the edge of each bluff body. In the CROM results, there are three categories of centroids represented. In centroids 1, 3, 6, 7, and 10, the two outer wakes oscillate in-phase, as a result of in-phase vortex shedding for those two wakes. These oscillations are more probable, as quantified by statistical analysis in Meehan *et al.* and as shown by the high-probability transfer areas in Figure 8. These centroids form a loop where the system spends much of its time, with smaller probabilities of transfer into other centroids. This dynamical loop seems to match the oscillations present in the first two modes of the POD, which together contain approximately 11 percent of the fluctuating energy in the flowfield.

For centroids 5, 8, and 9, the left wake and the center wake seem to be out of phase, where the oscillations in the center wake are coherent only in these centroids, although they are not nearly as strong as the oscillations in the two outer wakes in the first centroid group. These centroids form a secondary loop with centroid 6, which illustrates the pathway by which the flowfield can diverge from its most energetic loop (the 1-7-10-6-3 loop) and "mode switch" into a secondary loop of the 6-8-9-5 centroids. Centroid 6, therefore, acts as a switching point between these two oscillating modes. The structure of centroid 6 provides some clues as to the physics behind the switch from the more probable outer loop to the less probable inner loop. In the center wake in centroid 6, a small coherent oscillation appears (in red) approximately half-way down the field of view. In the outer loop, this center wake oscillation grows in strength in centroid 3 but is then merged or canceled with another oscillation in centroid 1, while the oscillations in the two outer wakes remain strong. This same oscillation in centroid 6 can also grow while the oscillations in the right wake weaken, as seen in the transition from centroid 6 to 8. This center-wake oscillation then grows and convects downstream in centroids 9 and 5 until the cycle begins again in centroid 6. This pattern suggests a physical reason for the intermittent switching, which is that oscillations in the center wake, approximately 1-2 diameters downstream of the bluff body, grow in strength and trigger more coherent oscillations downstream of this location. A similar intermittent switching process has been observed in dual-wakes in Ref. [15], although their explanation relied on a single events to describe the process. Here, we observe a statistically-significant event with some level of temporal resolution due to the time variations inherent in each centroid loop. Further, the oscillations present in this secondary loop are not captured in any one or pair of modes from the POD. This secondary loop and transition centroid (6) is only visible through the CROM analysis, and provides insight into the physics that drives the intermittent behavior of this flowfield.

Finally, centroids 2 and 4 represent random dynamics, where the phase for the different regions seems to be changing. These two centroids look similar to the transition centroids from the single-wake case, although the flowfield is much more complex in this multi-wake case. As they do not strongly connect with either the primary or secondary loop, and the centroids have no discernible structure, it is assumed that these motions are random motions that occur intermittently between the two "stable" loop behaviors.

The snapshot cluster assignments for the $w/D = 2.99$ case are shown in Figure 9. There is a stable region starting

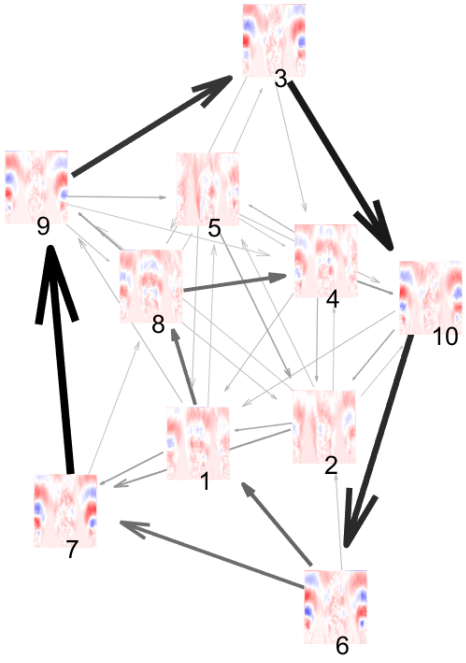

Fig. 8 Transition diagram with streamwise component of all cluster centroids for $w/D = 2.99$.

near 800 ms where the snapshots cycle through the five in-phase clusters (1-7-10-6-3). There are brief portions of the measurement near 500 ms and 1200 ms where the snapshots cycle through the three out-of-phase clusters (5-8-9). Finally, there are regions near 200 ms and 700 ms where the dynamics oscillate between the two remaining clusters (2 and 4). While the dynamics of this interacting flowfield are certainty intermittent, there is evidence of bistable behavior (1-7-10-6-3 and 6-8-9-5) separated by random behaviors (2 and 4).

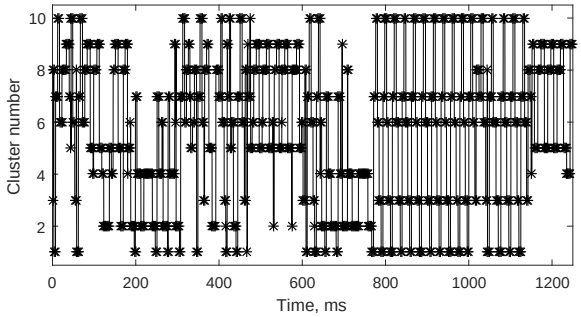

Fig. 9 Snapshot cluster assignments for three bluff body case, $w/D = 2.99$.

D. $w/D = 1.94$

We present the dynamics of the $w/D = 1.94$ case last because it shows how CROM responds to a flowfield with highly intermittent dynamics. The statistical analysis from Meehan *et al.* [17] showed that the oscillations between wakes in this intermediary spacing was almost completely random, where the distribution of the phase between wakes 1 and 3 was uniform across all phase angles. This type of flowfield challenges the CROM algorithm, as there may be very little coherence for it to identify. The streamwise components for the centroids in the $w/D = 1.94$ case are shown in Figure 10. An initial analysis of the transition diagram shows a highly complex loop that transitions between the following centroids with relatively high probability: 4-9-7-5-3-10-1-8-6-4. In this loop, the oscillations in the left wake are relatively stable, showing coherent motion and convection of those oscillations throughout the loop. However, there are significant fluctuations in the coherence of the center and right wakes. In the transition from centroids 4-9-7, the fluctuations in the center and right wakes grow in strength and coherence. In centroids 5-3-10, there is strong but out-of-phase shedding between the left and right wakes, as was seen in several other spacings. However, this coherence between the left and right wake does not last long, as in centroids 1-8-6, the coherence is lost before the cycle returns to centroid 4.

This cycle is one of many possibilities, however, as the probabilities of transition between centroids is highly distributed between paths. For example, the transitions from 4-9, 9-7, 7-5, 5-3, 3-10, and 10-1 are much stronger than any of the other options from each of those centroids. However, centroid 1 has two almost equally possible routes - one from 1-8, as in the cycle described before, or 1-5, where instead of the coherence in the right wake breaking down, the right wake strengthens again and continues to oscillate in the 5-3-10-1-5 loop. Centroid 1 therefore is an important switching point in the cycle, where now the strength of the coherent oscillations in the right wake is the deciding factor as to which path the system takes. Interestingly, the region where the disturbances gain or lose coherence is similar in the right wake of the $w/D = 1.94$ case and the central wake of the $w/D = 2.99$ case. This distance is approximately twice the vortex development length [31], and given its proximity to the end of the recirculation zone, may also be a highly sensitive region of the flow to external perturbations. Further adjoint analysis of this flowfield and its stability is recommended to understand the structural sensitivity of the flow and further understand why these switching points in the oscillation dynamics occur [11]. The cluster assignment time series is not as illuminating in this case as the oscillations are highly intermittent; as such, it is not included for brevity.

E. Discussion

The use of a cluster-based method for understanding the behavior of intermittent flowfields is highly encouraging. In particular, the CROM helped identify the most probable pathways for the flow dynamics and, more importantly, the points at which the flow bifurcates between possible paths. Using the structure of the centroids and how they develop along each "loop" has helped to identify sensitive regions of the flow and important physics that can *repeatably* result in

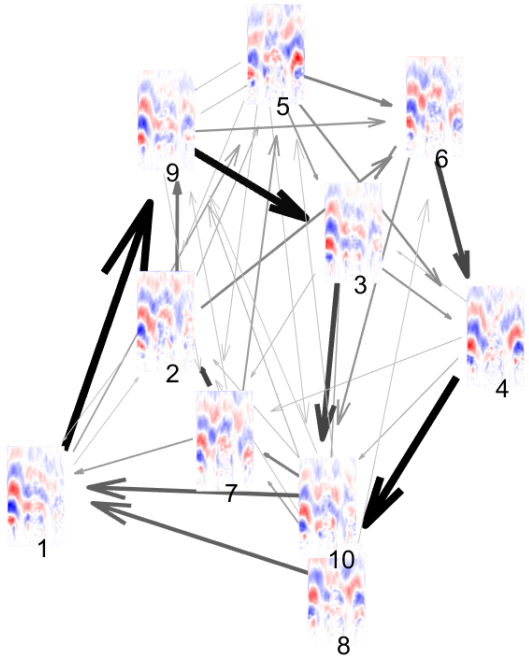

Fig. 10 Transition diagram of the streamwise component of all cluster centroids for $w/D = 1.94$.

changes in the flow behavior. While investigation of instantaneous dynamics is certainly illuminating and has lead to valuable insights in previous studies [10], the CROM technique provides information about both statistical significance as well as time-dependent behavior, which is a valuable contribution to understanding of flowfields that contain both coherent and random oscillations.

While the focus of this work has been on understanding the driving physics for behavioral switching in flows with high levels of intermittency, CROM also provides some metrics for quantifying the intermittency of a flowfield and comparing it with other flows. Several metrics for quantifying intermittency exist in the literature. Permutation entropy [32], which quantifies a conditional uncertainty of future data given the behavior of the data in the past, is a particularly useful method for identifying intermittency in signals. Commonly used in voice recognition software, permutation entropy is good at identifying coherent patterns that may intermittently occur in a time signal. Recurrence plots [33] have been used to illustrate the intermittency of a signal and provide a graphical means of identifying the "structure" of a signal. Both these methods, though, focus mainly on intermittency in one-dimensional signals, whereas it is more critical to be able to apply a quantification metric to spatially- and temporally-varying data like an intermittent flowfield as the intermittency is a function of both time and space.

One method of comparing the intermittency of the flowfield using the CROM is to compare the transition matrix for each of the data sets. The transition matrix entries, P_{jk}, are the probabilities of transition from cluster j to cluster k.

The probabilities of the diagonal, where $j = k$, are unity. If the off-diagonal entries are both sparse and high-probability, then the system exhibits limited intermittency as the variations between one centroid and the next are repeatable. The transition matrices for the single- and two three-wake cases are shown in Figure 11. The transition matrices in Figure 11 are ordered with increasing intermittency; the single-wake flowfield has the lowest level of intermittency and so the off-diagonal entries are sparse and have very high probabilities, showing the transitions between cluster 1 to 3, 3 to 4, 4 to 5, 5 to 2, and 2 back to 1. The transition matrices of the $w/D = 2.99$ and $w/D = 1.94$ cases have higher densities of entries off the diagnoal, where each entry has a lower probability than the entries in the single-wake case. While this view does not provide information about the order of the transitions, they provide a compact graphical representation of the intermittency of a spatiotemporally varying flowfield.

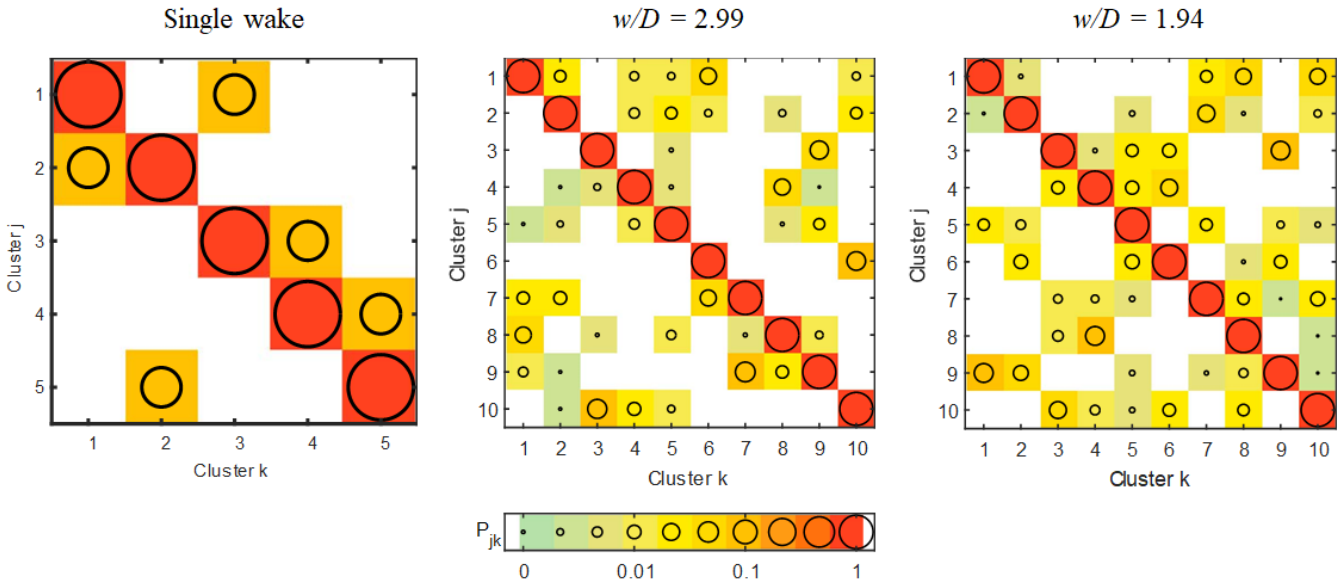

Fig. 11 Transition matrices for CROM analysis of single- and three-wake flows.

V. Conclusion

This study has shown that cluster-based reduced-order modeling can be used to understand the intermittent behavior of complex spatiotemporally varying flowfields. In this way, we can identify the mechanisms by which the flow switches modes using the transition diagrams and how probable each set of dynamics is using the transition matrices. These tools provide deeper insight into intermittency processes, whereas the tools of statistical analysis, used in a previous study [17], could not provide the physical insight that CROM does. Additionally, CROM provides statistically-significant, or repeatable, events and quantifies that repeatability using a transition probability, which provides added value over considering the instantaneous velocity fields and switching events one by one. This analysis technique has helped identify the region of the flowfield most sensitive to switching, which drives the transition from one oscillating mode to

another.

The results of this study will help us understand the structural sensitivity of interacting flows, opening avenues for design of control strategies in these flowfields. Specifically addressing closed-loop flow control, the use of CROM will address the intermittency, typically associated with larger Reynolds number, of nonlinear flows. Previous work combining stochastic estimation techniques with reduced-order modeling has proved to be successful in the context of closed-loop flow control [34]. The CROM could allow for real-time control of nonlinear flows, using the knowledge of the transition matrix to address the intermittency. While this might be considered a challenging goal, Kaiser *et al.* [35, 36] have already been able to use CROM to improve the open-loop actuation in a separating flow that is dominated by Kelvin-Helmholtz vortex shedding. Since this a strongly oscillatory flow, some further consideration would need to be investigated regarding flows with a high level of itermittency. The use of control with CROM for these applications is still being explored.

Funding Sources

This work was supported by the Air Force Office of Scientific Research under Grant FA9550-16-1-0075 with program manager Dr. Chiping Li.

Acknowledgments

The authors would like to acknowledge Ankit Tyagi for experimental support.

References

[1] Biermann, D., and Herrnstein, W., "The interaction between struts an cylinders in various combinations," *NACA Technical Report*, Vol. 468, 1933.

[2] Spivack, H. M., "Vortex frequency and flow pattern in the wake of two parallel cylinders at varied spacing normal to an air stream," *Journal of the Aeronautical Sciences*, Vol. 13, No. 6, 1946, pp. 289–301.

[3] Sumner, D., Wong, S., Price, S., and Paidoussis, M., "Fluid behaviour of side-by-side circular cylinders in steady cross-flow," *Journal of Fluids and Structures*, Vol. 13, No. 3, 1999, pp. 309–338.

[4] Le Gal, P., Chauve, M., Lima, R., and Rezende, J., "Coupled wakes behind two circular cylinders," *Physical Review A*, Vol. 41, No. 8, 1990, p. 4566.

[5] Le Gal, P., Peschard, I., Chauve, M., and Takeda, Y., "Collective behavior of wakes downstream a row of cylinders," *Physics of Fluids*, Vol. 8, No. 8, 1996, pp. 2097–2106.

[6] Kiya, M., Arie, M., Tamura, H., and Mori, H., "Vortex shedding from two circular cylinders in staggered arrangement," *Journal of Fluids Engineering*, Vol. 102, No. 2, 1980, pp. 166–171.

[7] Yen, S. C., and Liu, J. H., "Wake flow behind two side-by-side square cylinders," *International Journal of Heat and Fluid Flow*, Vol. 32, No. 1, 2011, pp. 41–51.

[8] Kim, H., and Durbin, P., "Investigation of the flow between a pair of circular cylinders in the flopping regime," *Journal of Fluid Mechanics*, Vol. 196, 1988, pp. 431–448.

[9] Bearman, P., and Wadcock, A., "The interaction between a pair of circular cylinders normal to a stream," *Journal of Fluid Mechanics*, Vol. 61, No. 3, 1973, pp. 499–511.

[10] Wang, Z., and Zhou, Y., "Vortex interactions in a two side-by-side cylinder near-wake," *International Journal of Heat and Fluid Flow*, Vol. 26, No. 3, 2005, pp. 362–377.

[11] Carini, M., Giannetti, F., and Auteri, F., "First instability and structural sensitivity of the flow past two side-by-side cylinders," *Journal of Fluid Mechanics*, Vol. 749, 2014, pp. 627–648.

[12] Carini, M., Giannetti, F., and Auteri, F., "On the origin of the flip–flop instability of two side-by-side cylinder wakes," *Journal of Fluid Mechanics*, Vol. 742, 2014, pp. 552–576.

[13] Carini, M., Auteri, F., and Giannetti, F., "Secondary instabilities of the in-phase synchronized wakes past two circular cylinders in side-by-side arrangement," *Journal of Fluids and Structures*, Vol. 53, 2015, pp. 70–83.

[14] Hayashi, M., Sakurai, A., and Ohya, Y., "Wake interference of a row of normal flat plates arranged side by side in a uniform flow," *Journal of Fluid Mechanics*, Vol. 164, 1986, pp. 1–25.

[15] Alam, M. M., Zhou, Y., and Wang, X., "The wake of two side-by-side square cylinders," *Journal of Fluid Mechanics*, Vol. 669, 2011, pp. 432–471.

[16] Zheng, Q., and Alam, M. M., "Intrinsic features of flow past three square prisms in side-by-side arrangement," *Journal of Fluid Mechanics*, Vol. 826, 2017, pp. 996–1033.

[17] Meehan, M., Tyagi, A., and O'Connor, J., "Flow dynamics in a variable-spacing, three bluff-body flowfield," *Physics of Fluids*, Vol. 30, No. 2, 2018, p. 025105.

[18] Lumley, J. L., "The structure of inhomogeneous turbulent flows," *Atmospheric Turbulence and Radio Wave Propagation*, 1967.

[19] Berkooz, G., Holmes, P., and Lumley, J. L., "The proper orthogonal decomposition in the analysis of turbulent flows," *Annual Review of Fluid Mechanics*, Vol. 25, No. 1, 1993, pp. 539–575.

[20] Sirovich, L., "Turbulence and the dynamics of coherent structures part I, II, III: coherent structures," *Q Applied Math*, Vol. 5, 1987, pp. 561–571.

[21] Willcox, K., and Peraire, J., "Balanced model reduction via the proper orthogonal decomposition," *AIAA Journal*, Vol. 40, No. 11, 2002, pp. 2323–2330.

[22] Rowley, C. W., "Model reduction for fluids, using balanced proper orthogonal decomposition," *Modeling And Computations In Dynamical Systems: In Commemoration of the 100th Anniversary of the Birth of John von Neumann*, World Scientific, 2006, pp. 301–317.

[23] Camphouse, R. C., Myatt, J., Schmit, R., Glauser, M., Ausseur, J., Andino, M., and Wallace, R., "A snapshot decomposition method for reduced order modeling and boundary feedback control," *4th Flow Control Conference*, 2008, p. 4195.

[24] Schmid, P. J., "Dynamic mode decomposition of numerical and experimental data," *Journal of Fluid Mechanics*, Vol. 656, 2010, pp. 5–28.

[25] Kaiser, E., Noack, B. R., Cordier, L., Spohn, A., Segond, M., Abel, M., Daviller, G., Östh, J., Krajnović, S., and Niven, R. K., "Cluster-based reduced-order modelling of a mixing layer," *Journal of Fluid Mechanics*, Vol. 754, 2014, pp. 365–414.

[26] Arthur, D., and Vassilvitskii, S., "k-means++: The advantages of careful seeding," *Proceedings of the eighteenth annual ACM-SIAM symposium on Discrete algorithms*, Society for Industrial and Applied Mathematics, 2007, pp. 1027–1035.

[27] Östh, J., Kaiser, E., Krajnović, S., and Noack, B. R., "Cluster-based reduced-order modelling of the flow in the wake of a high speed train," *Journal of Wind Engineering and Industrial Aerodynamics*, Vol. 145, 2015, pp. 327–338.

[28] Cao, Y., Kaiser, E., Borée, J., Noack, B. R., Thomas, L., and Guilain, S., "Cluster-based analysis of cycle-to-cycle variations: application to internal combustion engines," *Experiments in fluids*, Vol. 55, No. 11, 2014, p. 1837.

[29] Nasr, A., and Lai, J., "Comparison of flow characteristics in the near field of two parallel plane jets and an offset plane jet," *Physics of Fluids*, Vol. 9, No. 10, 1997, pp. 2919–2931.

[30] Williamson, C. H., "Vortex dynamics in the cylinder wake," *Annual review of fluid mechanics*, Vol. 28, No. 1, 1996, pp. 477–539.

[31] O'Connor, J., "Visualization of shear layer dynamics in a transversely forced flow and flame," *Journal of Propulsion and Power*, Vol. 31, No. 4, 2015, pp. 1127–1136.

[32] Bandt, C., and Pompe, B., "Permutation entropy: a natural complexity measure for time series," *Physical Review Letters*, Vol. 88, No. 17, 2002, p. 174102.

[33] Marwan, N., Romano, M. C., Thiel, M., and Kurths, J., "Recurrence plots for the analysis of complex systems," *Physics Reports*, Vol. 438, No. 5-6, 2007, pp. 237–329.

[34] Pinier, J. T., Ausseur, J. M., Glauser, M. N., and Higuchi, H., "Proportional closed-loop feedback control of flow separation," *AIAA journal*, Vol. 45, No. 1, 2007, pp. 181–190.

[35] Kaiser, E., Noack, B. R., Spohn, A., Cattafesta, L. N., and Morzyński, M., "Cluster-based control of a separating flow over a smoothly contoured ramp," *Theoretical and Computational Fluid Dynamics*, Vol. 31, No. 5-6, 2017, pp. 579–593.

[36] Kaiser, E., Morzyński, M., Daviller, G., Kutz, J. N., Brunton, B. W., and Brunton, S. L., "Sparsity enabled cluster reduced-order models for control," *Journal of Computational Physics*, Vol. 352, 2018, pp. 388–409.